IRAQI JOURNAL OF MATERIALS
Volume (5) Issue (2) April-June 2026, pp. 77-84
Published and Sponsored by American Quality for Scientific Publishing, Inc. (AQSP)

Photoluminescence Characterization of $CuInS_2$ Quantum Dots Incorporated in Hybrid Structures for Light Emission Devices

René Ramón, Layla Daleel*, Martha S. Fiddler

Department of Physics, Faculty of Science, University of Piraeus, Piraeus, GREECE
** Corresponding author email: daleel.nano@gmail.com*

Abstract
In this work, hybrid multilayer structures containing $CuInS_2$ quantum dots coated with ZnMgO shells and incorporated in conductive polymeric matrices (PEDOT:PSS and TFB) were prepared and characterized to develop eco-friendly toxic-free light emitting devices. Results showed that addition of formamidinium acetate (FAAc) lead to enhance the microstructure by reducing the agglomerations and surface roughness to support the homogeneity and connection of the grains. The existence of all organic and inorganic constituents was confirmed with dominant carbon bonds distinguishing the polymeric layers. The photoluminescence (PL) spectroscopy revealed a reasonable enhancement in the intensity of the emitted light as well as a slight redshift due to treatment with FAAc. The electrical characteristics showed the behavior of negative differential resistance at high voltages due to heating and charge collection effects at the interfaces. A maximum value of external quantum efficiency (EQE) of 10% was achieved at applied voltage of 6.5 V as the radiative recombination dominates. These results reveal that the FAAc-treated hybrid structures show promising optoelectronic characteristics for low-cost light emitting devices with high color purity and stable performance at high voltages.

Keywords: Quantum dots; Hybrid structures; $CuInS_2$; Photoluminescence
Received: November 2025; **Revised:** January 2026; **Accepted:** February 2026; **Published:** April 2026

1. Introduction

The $CuInS_2$ quantum dots are described as ternary semiconductor (I-III-VI) with adjustable energy bandgap depending on size and chemical structure. The fundamental feature of these materials is they are toxic-free of elements such as cadmium lead, which makes them eco-friendly. The photoluminescence (PL) mechanism of these quantum dots mainly depends on the sub-bandgap transitions due to point defects, such as copper vacancies or interstitial copper atoms. This behavior lead to large Stokes shift that reduces the self-absorption, which is an important feature to enhance the efficiency of light emitting devices [1-4]. The quantum confinement effect contributes to enhance the quantum yield throughout charge carriers trapping at the nanoscale that increase the probability of radiative recombination [5-7].

The hybrid structures have significantly advanced the design of light-emitting devices as the quantum dots were incorporated in polymeric or inorganic matrices to enhance the photochemical stability [8]. In such systems, the interfaces play a crucial role in charge injection and nonradiative energy transfer processes [9]. The efficiency of the hybrid device reasonably depends on the energy level alignment of the donor and acceptor materials, especially the highest occupied molecular orbit (HOMO) and lowest unoccupied molecular orbit (LUMO). This alignment assists in reducing the phenomenon of exciton quenching as well as enhancing the excited state lifetime [10-12]. Moreover, the hybrid structures can provide mechanical protection for the quantum dots against the photo-oxidation, which guarantees sustainable spectroscopic performance when operated continuously with high electric current [13-15].

The photoluminescence characterization is the much more accurate analytical tool to understand the dynamics of charge carriers within the hybrid nanostructures. By analyzing the emission spectrum, the full-width at half maximum (FWHM) can be determined to show the size monodispersity of these nanoparticles [16-18]. Also, the time-resolved photoluminescence (TRPL) technique provides a deep insight about emission mechanism since it allows measuring the fluorescence decay time and distinguishing between surface and bulk recombination processes. These measurements are important to evaluate the energy transfer efficiency in the hybrid structure and determine the effectiveness of the surface passivation by the chemical ligands [19-21]. Linking the experimental data of photoluminescence to the structural characteristics prepares to enhance the light extraction efficiency and hence develop light sources of high color purity at low production cost [22,23].

The semiconducting nanoparticles or quantum dots are an exceptional type of nanomaterials those made a revolution in the optoelectronics due to their unique optical and electronic properties, originate from the quantum confinement effect where the excitons are confined within dimensions smaller than Bohr radius of the material [24]. This confinement leads to splitting energy levels into sub-levels, so the nanoparticle energy bandgap sufficiently depends on its size. Consequently, the color of the emitted light can be accurately adjusted by controlling the quantum dot size during the formation process [25]. Amongst semiconducting materials widely used in this field, copper indium disulfide ($CuInS_2$) represents a promising eco-friendly candidate free of toxic elements. It has a direct energy bandgap in the visible and near-infrared (NIR) that makes it optimum selection in solar cells, light-emitting devices, and biosensing applications [26-28].

Despite the potential advantages of the $CuInS_2$ quantum dots, their effective employment in optical and photonic devices requires solving the challenges related to their stability and quantum yield. The bare quantum dots mostly suffer from the surface defects that work as nonradiative recombination centers, which reduce the photoluminescence efficiency [29,30]. To overcome this limitation, the quantum dots are incorporated into the hybrid structures to prepare a protective host for these quantum dots, enhance the charge transfer, and support the thermochemical stability [31]. The proposed strategies include coating of the quantum dots with inorganic shells from another semiconducting material with larger energy bandgap (such as ZnO) to form core/shell structures. This shell effectively isolates the core from the surrounding environment, passes electrons and holes towards the core, increases the probability of radiative recombination, and hence significantly support the photoluminescence efficiency [32-34]. Furthermore, the quantum dots can be dispersed within a conductive or dielectric polymeric matrix to provide mechanical support and allow low-cost solution processability in order to fabricate large-scale devices with controlled design to enhance the charge transfer to the electrodes of the functional devices [35-37].

In this work, $CuInS_2$ quantum dots were incorporated into polymeric matrices to form hybrid structures and their optical, electronic, and spectroscopic characteristics were introduced to show their feasibility for specific applications, mainly, light-emitting devices.

2. Experimental Part

To fabricate the hybrid structure shown in Fig. (1), the PEDOT:PSS (Poly(3,4-ethylenedioxythiophene) polystyrene sulfonate) solution was prepared and filtered with 0.5μm-porosity filtering paper to ensure the structural purity of the prepared layer. As well, the TFB (Poly(9,9-dioctylfluorene-alt-N-(4-sec-butylphenyl)-diphenylamine)) solution by dissolving 8 mg in 1 mL of chlorobenzene with stirring at temperature of 50 °C for two hours to ensure complete dissolving and homogeneity. The $CuInS_2$ quantum dots coated with ZnO shell and dispersed in toluene at a concentration of 10 mg/mL. A specific amount of zinc-doped magnesium oxide (ZnMgO) was dispersed in ethanol at a concentration of 30 mg/mL. All solutions were kept in desiccators in dry nitrogen to avoid any degradation in their photochemical characteristics.

The multilayer structures were formed on indium-doped tin oxide (ITO) substrates. These substrates were thoroughly cleaned by ultrasonic waves, rinsed in acetone and isopropanol, and dried with nitrogen gas flow. The spin coating method was used to deposit the multilayer structure layer by layer. First, the PEDOT:PSS layer was deposit at 4000 rpm for 30 seconds and then heated up to 120 °C for 10 minutes to remove the solvent. Second, the TFB layer was deposited at 2000 rpm for 30 seconds and then heated up to 150 °C for 20 minutes. Third, a layer of $CuInS_2$ quantum dots was deposited at 1500 rpm for 30 seconds and then slowly heated up to 80 °C for 3 minutes to keep the stability. Finally, a layer of ZnMgO was deposited at 2000 rpm for 30seconds and then heated up to 80 °C for 10 minutes. The deposition conditions were accurately controlled to produce homogeneous and surface defect-free layers. In order to perform the optoelectronic measurements on the prepared hybrid structures, silver paint was used to make front electrode over the top ZnMgO layer. The formamidinium acetate (FAAc) was added to the $CuInS_2$ solution as it modulates precursor chemistry by forming complexes that control the size and bandgap of the resulting nanocrystals, without significantly altering their crystal structure.

The photoluminescence spectra were recorded using a dual-beam computerized spectrophotometer supplied with various lasers (405, 430, 530, 630, and 850nm) as excitation sources. The emission spectra were recorded in the spectral range of 400-800 nm at room temperature. The Fourier-transform infrared (FTIR) spectroscopy was carried out using a Shimadzu spectrometer, the surface morphology was introduced by the scanning electron microscopy (SEM), while the electrical (current-voltage) characteristics were determined using a dc power supply and microammeter.

IRAQI JOURNAL OF MATERIALS
Volume (5) Issue (2) April-June 2026, pp. 77-84
Published and Sponsored by American Quality for Scientific Publishing, Inc. (AQSP)

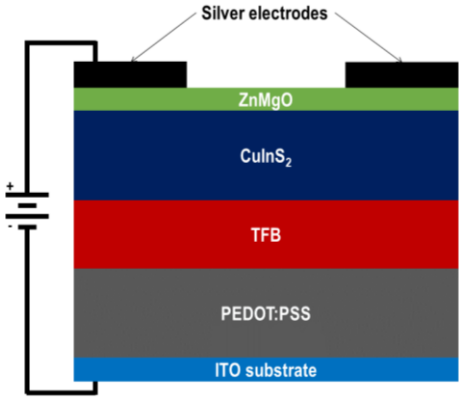

Fig. (1) Schematic diagram of the multilayer structure fabricated in this work

3. Results and Discussion

Figure (2) shows the FTIR spectrum of the $CuInS_2$ QDs with the FAAc additive. This spectrum shows distinct absorption peaks revealing the chemical structure of the prepared multilayers. Within the spectral range of 1350-1450 cm^{-1}, the vibration peaks are ascribed to the bending mode of C-H bonds in the organic (PEDOT:PSS) compounds that contain conductive polymers as well as in the TFB layer that contains polymers of aromatic units [38]. These peaks confirm the existence of carbon chains within these layers. In the range of 1500-1600 cm^{-1}, absorption peaks related to the vibrations of the aromatic ring (C=C) in both PEDOT:PSS and TFB, which further confirms the existence of the conductive polymers [39]. In the range of 1650-1750 cm^{-1}, the peaks are attributed to the vibrations of the C=O bonds, which may result from the humidity adsorbed by or slight surface oxidation on the PEDOT:PSS layer or due to the precursors used to prepare these layers [40]. In the range of 2850-2950 cm^{-1}, the absorption peaks ascribed to the stretching modes of the C-H bonds are observed to reveal the existence of the alkyl side chains in the TFB [41].

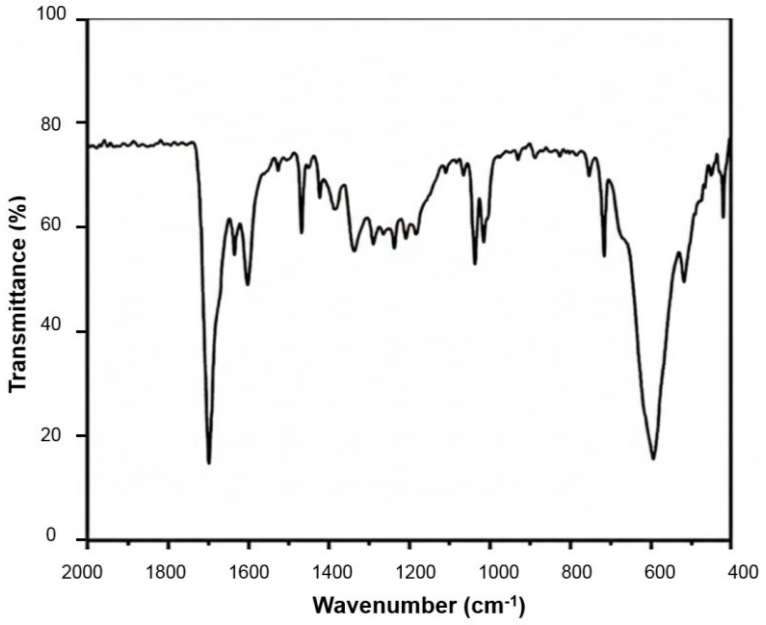

Fig. (2) FTIR spectrum of the Ag/ZnMgO/$CuInS_2$/TFB/PEDOT:PSS/ITO structure with FAAc additive

It is important to observe that some peaks in the range of 1000-1200 cm^{-1} may be attributed to the vibrations of S=O and C-O-C bonds in the PEDOT:PSS, which confirms the formation of this layer [42]. Despite that the $CuInS_2$ and ZnMgO layers are fundamentally inorganic, their effects on the spectrum

may be limited in the region below 1000 cm^{-1} as the vibrations of the metal-oxygen (M-O) or metal-sulfur (M-S) bonds appear but may partially be blocked due to the absorption of the organic layers or the interference with the absorption of silver (front electrode), which may support some absorption peaks due to the surface amplification but not change the positions of the peaks [43]. In general, the FTIR spectrum reveals the proposed multilayer structure with apparent dominant vibrations of the organic PEDOT:PSS and TFB layers, while the inorganic layers show smaller contributions.

Figure (3) shows the SEM images of the $CuInS_2$ QDs without and with the FAAc additive, whose effect on the morphology of the $CuInS_2$ QDs is apparent. The surface of the $CuInS_2$ QDs (Fig. 3a) shows grains or clusters with relatively apparent boundaries with grain size in the range of 10-30 nm. The surface seems dense but apparent agglomerations are observed, which refers to a conventional crystalline grown of $CuInS_2$ QDs with differences in the particle size distribution. This structure may lead to huge number of grain boundaries that work as recombination centers of charge carriers in photonic devices, such as solar cells and photonic sensors, which may reduce the their efficiencies.

In the second image (Fig. 3b) of the $CuInS_2$ QDs with FAAC additive, a radical variation in the surface morphology is observed as the surface shows lower roughness, much more homogeneity, and observable smaller agglomerations. The grains seem denser and better connected due to the role of FAAc as a passivation agent during the preparation process. It reduces the reaction rate or control the crystalline growth to produce reasonably uniform grains. The addition of FAAc to the $CuInS_2$ QDs solution may enhance the wettability of the precursors on the substrate or assist in removing the organic impurities during crystallization to produce cleaner and denser surface [44]. The final result is the formation of $CuInS_2$ layer with higher surface quality, fewer large vacancies and structural defects, and hence better optical and electronic properties of the material. Accordingly, it can be said that the addition of FAAc reasonably enhances the microstructure and then makes the material much more suitable for the applications requiring effective transfer of charge carriers and improved photonic response.

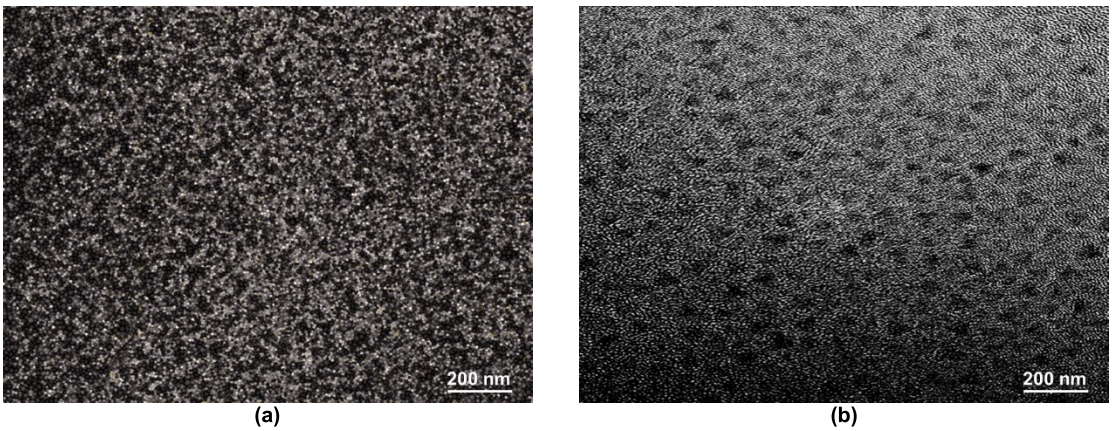

(a) (b)

Fig. (3) SEM images of $CuInS_2$ QDs (a) and $CuInS_2$ with FAAc additive (b)

Figure (4) shows the photoluminescence (PL) spectra of the $CuInS_2$ QDs without and with the FAAc additive. The $CuInS_2$ QDs shows relatively weak absorption peak at 690 nm due to a high level of the nonradiative recombination due to surface defects or large grain boundaries that work as trapping centers for the charge carriers, which reduces the PL efficiency. The relative broadening of the spectrum refers to a broad distribution of energy states resulted from the structural defects. On the other hand, the PL spectrum of the $CuInS_2$ QDs with FAAc shows drastic enhancement in the intensity with a peak shifted to 710 nm. This dramatic enhancement confirms that the addition of FAAc have reasonably improved the crystalline structure and reduced the nonradiative defects, as revealed by the SEM images. The shift in the peak (~20 nm) means that the nature of fundamental electronic transition in the material was not chemically affected, i.e., the FAAc did not reasonably change the energy bandgap of the $CuInS_2$ QDs, instead, it enhances the radiative efficiency throughout surface passivation. The drop of the spectrum beyond the peak became sharper due to narrower distribution of the grains and much more uniform in energy states. The tail in the spectrum of the $CuInS_2$ QDs with FAAc beyond 900 nm may refer to electronic transitions related to shallow surface states or residual defects, but their relatively low intensity confirms that the recombination mostly occurs along direct radiative path.

IRAQI JOURNAL OF MATERIALS
Volume (5) Issue (2) April-June 2026, pp. 77-84
Published and Sponsored by American Quality for Scientific Publishing, Inc. (AQSP)

Figure (5) shows the electroluminescence (EL) spectra of the $CuInS_2$ QDs with FAAc additive for three different values of the operating voltage (5, 10, and 15 V) as the sufficient dependence on the operating voltage reveals the recombination dynamics in these nanostructures. At low voltage (6 V), the intensity of the EL spectrum is low with a peak at 725 nm, which means that the carrier injection is relatively weak and the produced radiation originates solely from recombination from the regions of higher efficiency or the radiative centers of lower energy. Increasing the voltage to 10 V has resulted in more than 6 times increase in the intensity while the peak was not shifted from 725 nm with slight broadening in the spectrum width due to the increase in the density of injected charge carriers and the activation of more radiative recombination centers. The further increase in the intensity (~150%) with increasing the voltage to 15 V refers to exceeding a specific threshold by the charge carriers injection as the majority of injected electrons and holes tend to radiative recombination instead of dissipating in nonradiative paths. As well, the peak position was not changed that confirms that the electroluminescence (EL) originates from the same fundamental electronic transition in $CuInS_2$ and the FAAc has enhanced the efficiency of this transition with no change in its nature. The extended spectrum at wavelength longer than 800 nm may be attributed to contributions from surface states or shallow defects those are activated at higher injection rates, however, the low intensity reveals that most radiation is produced by the direct transition through the energy bandgap.

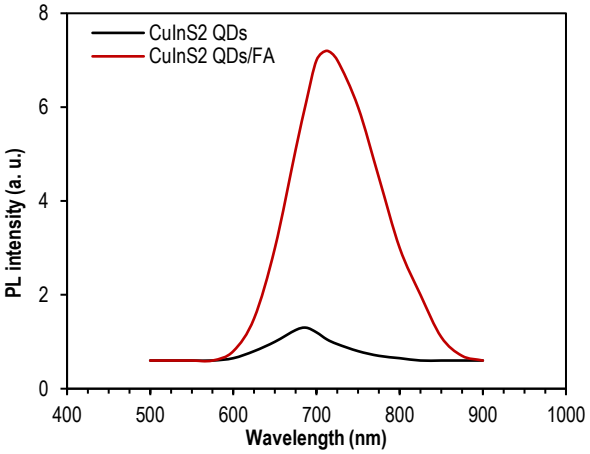

Fig. (4) PL spectra of the $CuInS_2$ QDs with and without FAAc additive

The observed symmetry in all spectra at all voltages refers to a stability in the recombination mechanism and an absence of thermal effects or material degradation at high voltages. Unshifted emission peak with increasing voltage (no Stark effect) reveals that the internal electric field in the structure does not reasonably deform the energy states, which confirms the quality of the interfaces between the layers as well as the passivation effect of the FAAc additive in reducing the density of confined charges.

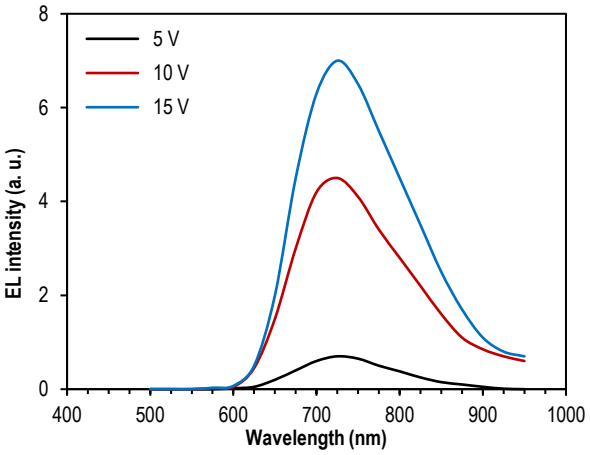

Fig. (5) EL spectra of $CuInS_2$ QDs with FAAc additive at three different values of operating voltage

IRAQI JOURNAL OF MATERIALS
Volume (5) Issue (2) April-June 2026, pp. 77-84
Published and Sponsored by American Quality for Scientific Publishing, Inc. (AQSP)

Figure (6) shows the current-voltage characteristics of the multilayer structure fabricated in this work as a light emitting device. At low applied voltages (4-4.5 V), no current was flowing in the device as the charge carriers (electrons and holes) did not have sufficient energy to overcome the potential barriers at the interfaces. Within the variation of voltage from 4.5 to 6 V, the current exhibited a sharp linear increase as this range represents the efficient initial carrier injection and reached a maximum value of 29 mA/cm^2 at applied voltage of 7 V, which can be considered as the optimum operation point of this device. Beyond this point, the current gradually decreased to reach an approximately constant value of 16 mA/cm^2 during the range of 9-10 V. This behavior refers to a phenomenon known as "negative differential resistance" and the reduction in the current is usually attributed to the effects of Joule heating, which changes the conduction characteristics of organic materials (PEDOT:PSS and TFB) or to the intense carrier recombination that reduced their lifetime and effective mobility. As well, the existence of absorbing layer ($CuInS_2$) and blocking layer (ZnMgO) may lead to charge accumulation at the interfaces under strong fields to prevent current flow. In general, these characteristics reveal good performance of the fabricated device in the voltage range from 6 to 8 V, but they show the challenges of thermal stability and injection balance at higher voltages. These characteristics are important in designing solar cells and light emitting diodes.

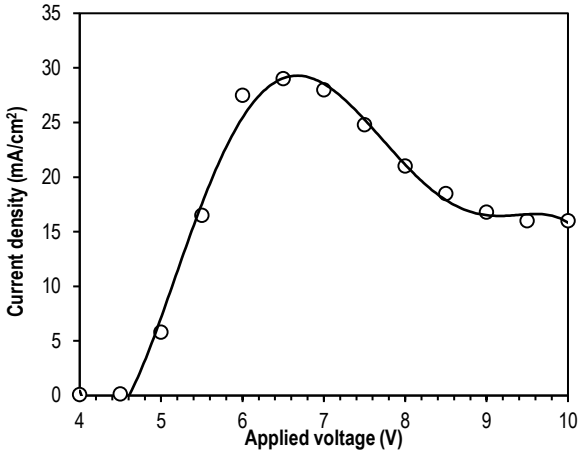

Fig. (6) Current-voltage characteristics of multilayer structure fabricated in this work

Figure (7) shows the variation of external quantum efficiency (EQE) of the multilayer structure fabricated in this work with the applied voltage. The behavior of the $CuInS_2$ QDs treated with FAAc reveals complex dynamics of the current-to-light conversion by the fabricated device. The EQE is very low at low voltage (<5.5V) as the charge carriers injection still below the threshold required to initiate the effective radiative recombination as the nonradiative processes reasonably dominate. The EQE increases sharply with increasing applied voltage beyond 5.5 V as the operation threshold is exceeded and the injected charge carriers started to overcome the traps and defects. The highest value of EQE (~10%) is determined at 6.5 V can be exceptional result to confirm the high quality of the $CuInS_2$ QDs treated with FAAc. Beyond this peak, the EQE gradually decreases with increasing applied voltage and this phenomenon is known efficiency roll-off, which occurs when the charge carrier density becomes very high and the nonradiative recombination processes (Auger) dominates, or when the heating resulted from high current flow that increases the lattice vibrations (phonons) and hence the energy loss. The FWHM of about 1 V refers to a relatively stable operation range of the fabricated device.

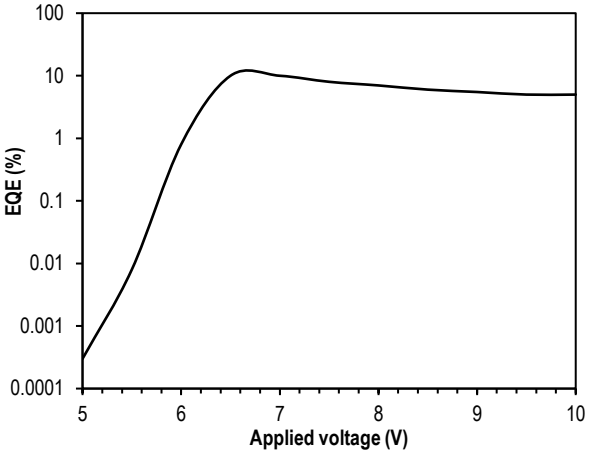

Fig. (7) Variation of EQE with applied voltage for multilayer structure fabricated in this work

4. Conclusions

In concluding remarks, the addition of FAAc to the $CuInS_2$ QDs leads to passivate surface defects and hence enhance the microstructure of the hybrid structures based on these nanostructures incorporated in polymeric matrices. Consequently, the PL intensity is enhanced and its peak is shifted by 20nm without changing the energy bandgap of the active nanostructures. The negative differential resistance and efficiency reduction were observed at high applied voltages due to heating effects and dominance of Auger recombination process. These results confirm the effectiveness and feasibility of the fabricated hybrid structures in the applications of eco-friendly light emitting devices.

References

[1] M. Michalska et al., "Amine ligands control of the optical properties and the shape of thermally grown core/shell $CuInS_2$/ZnS quantum dots", *J. Alloys Comp.*, 645 (2015) 184-192.
[2] A. Moudgil et al., Chapter 8 - Quantum dots based vehicles for controlled drug release in conjunction with bio-imaging, V. Gajbhiye, K.R. Gajbhiye, S. Hong (eds.), Stimuli-Responsive Nanocarriers, Academic Press (2022), pp. 197-236, ISBN 9780128244562.
[3] S. Tian et al., "Reaction engineering studies of the continuous synthesis of $CuInS_2$ and $CuInS_2$/ZnS nanocrystals", *Chem. Eng. J.*, 289 (2016) 365-373.
[4] Z. Wang and M. Tang, "The cytotoxicity of core-shell or non-shell structure quantum dots and reflection on environmental friendly: A review", *Environ. Res.*, 194 (2021) 110593.
[5] A. Rahman, J.R. Jennings, and M.M. Khan, "$CuInS_2$ and CuInS2-based nanostructures as photocatalysts", *Mater. Sci. Semicond. Process.*, 169 (2024) 107930.
[6] U. Abdullah, M. Ali, and E. Pervaiz, "An Inclusive Review on Recent Advancements of Cadmium Sulfide Nanostructures and its Hybrids for Photocatalytic and Electrocatalytic Applications", *Mole. Catal.*, 508 (2021) 111575.
[7] R. Banyal et al., "Emergence of $CuInS_2$ derived photocatalyst for environmental remediation and energy conversion", *Environ. Res.*, 238(2) (2023) 117288.
[8] J. Wang et al., "Fluorescent/luminescent detection of natural amino acids by organometallic systems", *Coordin. Chem. Rev.*, 303 (2015) 139-184.
[9] Y.-Y. Ren et al., "Host-guest assemblies of anchoring molecular catalysts of CO_2 reduction onto $CuInS_2$/ZnS quantum dots for robust photocatalytic syngas production in water", *Mole. Catal.*, 520 (2022) 112168.
[10] W. Yue et al., "Different depositing amount of $CuInS_2$ on TiO_2 nanoarrays for polymer/$CuInS_2$–TiO_2 solar cells", *Mater. Sci. Semicond. Process.*, 40 (2015) 257-261.
[11] H. Muhammad et al., "A comprehensive review of current trends and future perspective of quantum dots regarding their optical and photoswitchable properties", *Renew. Sustain. Energy Rev.*, 223 (2025) 115984.
[12] M. Ye et al., "Multifunctional quantum dot materials for perovskite solar cells: Charge transport, efficiency and stability", *Nano Today*, 40 (2021) 101286.
[13] N.S.M. Mustakim et al., "Quantum dots processed by SILAR for solar cell applications", *Solar Energy*, 163 (2018) 256-270.
[14] C. Cai et al., "Tailoring defects of $CuInS_2$ quantum dots for sensitized solar cells", *J. Alloys Comp.*, 719 (2017) 227-235.
[15] W. Yue, M. Wang and G. Nie, "Ternary MEH-PPV-$CuInS_2$/ZnO solar cells with tunable $CuInS_2$ content", *Solar Energy*, 99 (2014) 126-133.
[16] S. Jindal et al., "Green synthesis of $CuInS_2$/ZnS core-shell quantum dots by facile solvothermal route with enhanced optical properties", *J. Phys. Chem. Solids*, 114 (2018) 163-172.
[17] P. Sharma et al., "Current scenario in ternary metal indium sulfides-based heterojunctions for photocatalytic energy and environmental applications: A review", *Mater. Today Commun.*, 36 (2023) 106741.
[18] O.S. Oluwafemi et al., Chapter Four - Ternary semiconductor nanocomposites, O.S. Oluwafemi, E.H.M. Sakho, S. Parani, T.C. Lebepe, in Woodhead Publishing Series in Electronic and Optical Materials, Ternary Quantum Dots, Woodhead Publishing (2021), pp. 77-115, ISBN 9780128183038.
[19] B. Gidwani et al., "Quantum dots: Prospectives, toxicity, advances and applications", *J. Drug Deliv. Sci. Technol.*, 61 (2021) 102308.

[20] M. Zhou, S. Zhang, and Y. Wang, "ZnS-shelled and Zn-doped $CuInS_2$ quantum dots for TiO_2-based UV photodetectors", *Chem. Phys. Lett.*, 862 (2025) 141861.
[21] N. Thondavada et al., 15 - New generation quantum dots as contrast agent in imaging, S. Kanchi, D. Sharma (eds.), Nanomaterials in Diagnostic Tools and Devices, Elsevier (2020), pp. 417-437, ISBN 9780128179239.
[22] B. Xia et al., "Differential effects of PEGylated Cd-free $CuInS_2$/ZnS quantum dot (QDs) on substance P and LL-37 induced human mast cell activation", *Ecotoxicol. Environ. Safety*, 245 (2022) 114108.
[23] J. Zhang et al., "Copper indium sulfide quantum dots in photocatalysis", *J. Colloid Interface Sci.*, 638 (2023) 193-219.
[24] O. Cavdar et al., "Remarkable visible-light induced hydrogen generation with $ZnIn_2S_4$ microspheres/$CuInS_2$ quantum dots photocatalytic system", *Int. J. Hydrogen Ener.*, 46(1) (2021) 486-498.
[25] M.A. Mimona et al., "Quantum dot nanomaterials: Empowering advances in optoelectronic devices", *Chem. Eng. J. Adv.*, 21 (2025) 100704.
[26] N. Poornima et al., "Composition and Conductivity-type Analysis of Spray Pyrolysed ZnS Thin Films using Photoluminescence", *Energy Procedia*, 15 (2012) 347-353.
[27] M.A. Raheem et al., "Advances in nanoparticles-based approaches in cancer theranostics", *OpenNano*, 12 (2023) 100152.
[28] K. Wang et al., "Chemical stoichiometry and gradient shell engineering for highly-efficient narrow near-band-edge emission in $CuInS_2$ quantum dots", *Nano Mater. Sci.*, 8(1) (2026) 59-68.
[29] Y. Qin et al., "Colloidal $CuInS_2$ quantum well nanostructures with II–VI semiconductors as barrier layers", *Chem. Sci.*, 16(22) (2025) 10051-10060.
[30] S. Soman et al., "Bioinspired quantum dots: advancing diagnostic and therapeutic strategies in breast cancer", *RSC Adv.*, 15(34) (2025) 27738-27771.
[31] V. Sahu and S.K. Sahoo, "Percutaneous permeation, distribution and absorption of quantum dots", *Next Nanotech.*, 9 (2026) 100368.
[32] M. Inada et al., "Effect of the indium sulfide phase in $CuInS_2$-TiO_2 photocatalysts to boost hydrogen evolution by water splitting", *Mater. Today Catal.*, 7 (2024) 100080.
[33] E.P.J. Merkx, M.P. Plokker, and E. van der Kolk, "The potential of transparent sputtered NaI:Tm^{2+}, $CaBr_2$:Tm^{2+}, and CaI_2:Tm^{2+} thin films as luminescent solar concentrators", *Sol. Ener. Mater. Solar Cells*, 223 (2021) 110944.
[34] C. Zhu et al., "Recent advances in non-toxic quantum dots and their biomedical applications", *Prog. Nat. Sci.: Mater. Int.*, 29(6) (2019) 628-640.
[35] S.-K. Ming et al., "Tunable structural and optical properties of $CuInS_2$ colloidal quantum dots as photovoltaic absorbers", *RSC Adv.*, 11(35) (2021) 21351-21358.
[36] M. Oda et al., "Synthesis, Characterization and its Photoluminescence Properties of Group I-III-VI2 $CuInS_2$ nanocrystals", *Phys. Procedia*, 29 (2012) 18-24.
[37] L.A. Ramolise et al., "Recent advances on visible and near-infrared thermometric phosphors with ambient temperature sensitivity: A review", *Coordin. Chem. Rev.*, 522 (2025) 216196.
[38] P. Tandale et al., "Fluorescent quantum dots: An insight on synthesis and potential biological application as drug carrier in cancer", *Biochem. Biophys. Rep.*, 26 (2021) 100962.
[39] S.I. Mohammad et al., "Pioneering perovskite quantum dot nanosensors for heavy metal ion detection: mechanisms, design, and industrial applications", *RSC Adv.*, 15(48) (2025) 40338-40367.
[40] D. Voigt, M. Bredol, and A. Gonabadi, "A general strategy for $CuInS_2$ based quantum dots with adjustable surface chemistry", *Opt. Mater.*, 115 (2021) 110994.
[41] J. Patil and S. Bhattacharya, "Exploring the potential of quantum dots and plasmonic nanoparticles for imaging and phototherapy in colorectal neoplasia", *Result. Chem.*, 10 (2024) 101689.
[42] S. Castelletto and A. Boretti, "Luminescence solar concentrators: A technology update", *Nano Energy*, 109 (2023) 108269.
[43] S. Sargazi et al., "Fluorescent-based nanosensors for selective detection of a wide range of biological macromolecules: A comprehensive review", *Int. J. Biol. Macromol.*, 206 (2022) 115-147.
[44] A. Sadeqi et al., "Hybrid microneedle patch for administration of measles and rubella vaccine with an on-patient medical record", *J. Control. Release*, 391 (2026) 114635.

